Adiabatic Mode-Matching Techniques for Coupling Between Conventional Microwave Transmission Lines and One-Dimensional Impedance-Interface Waveguides

Zhixia Xu, Xiaoxing Yin, and Daniel F. Sievenpiper

Phys. Rev. Applied **11**, 044071 — Published 22 April 2019

DOI: 10.1103/PhysRevApplied.11.044071

Adiabatic mode-matching techniques for coupling between conventional microwave transmission lines and one-dimensional impedance-interface waveguides

Zhixia Xu[1,2], Xiaoxing Yin[1], and Daniel F. Sievenpiper[2]

1 State Key Laboratory of Millimeter Waves, Southeast University, Nanjing 210096, China
2 Electrical and Computer Engineering Department, University of California, San Diego, California 92093, USA

Zhixia Xu: 230159363@seu.edu.cn;
Xiaoxing Yin: 101010074@seu.edu.cn;
Daniel F. Sievenpiper: dsievenpiper@eng.ucsd.edu.

Waveguides consisting of artificial media based on periodic structures at the subwavelength scale are a major open topic in contemporary applied physics and engineering. Recent research efforts focus on properties of guided modes in artificial structures. However, as the cornerstone of applications, matching techniques between these interesting waveguides and traditional waveguides deserve more attention. We report a broadband adiabatic mode matching technique for efficient coupling between conventional microwave transmission lines (a coplanar waveguide and a slotline) and one-dimensional (1D) interface waveguides consisting of transverse-electric (TE) and transverse-magnetic (TM) artificial impedance surfaces. The transverse electromagnetic (TEM) mode is transformed to the line wave mode at the 1D impedance-interface adiabatically. Proposed matching techniques open up an avenue for applications of various impedance-interface waveguides.

INTRODUCTION

As solutions of Maxwell's equations, guided waves at the interface of two different materials which decay away from the interface have been studied for decades [1]. Surface plasmons, Dyakonov-Tamm waves, and Zenneck waves can all be treated in a unified form [2, 3]. With a peak field bound at the interface, these waves are attractive for communication and sensing applications [4]. In order to utilize waves at interfaces of different media, various waveguides have been invented. Goubau lines [5–7], as well as spoof surface plasmons [8–11], support waves at the interface of metals and dielectrics. Dielectric waveguides [12, 13], such as fibers, support waves at the interface of dielectrics with different permittivity. Based on the concept that the local intensity of guided waves

can control the wavevector, nonlinear waveguides have been attractive for decades for their multiplicity of applications to all-optical signal processing systems [14–17]. Photonic crystals support waves along the interface of two photonic crystals with overlapping band gaps [18, 19]. Topological insulators support waves at the interface of trivial and non-trivial materials in topological space [20, 21]. In the past several years, researchers have found a different one-dimensional (1D) impedance-interface mode, called a line wave (LW) mode, at the interface of two planes with different surface impedances from microwave to optical bands [22–24]. Further researches focusing on similar waveguides were reported recently [25, 26]. LW modes show robustness with wave-vector-locked states as well as field confinement ability. Compared to photonic crystals based on overlapping narrow energy gaps, LW modes have a very broadband transmission feature. However, this also brings a drawback: without overlapped bandgaps, surface waves can propagate in any direction on the two surrounding impedance surfaces. Thus, it is difficult to excite a pure LW mode with suppressed surface waves on both sides. Previous methods to excite and detect the LW mode were based on probes fabricated at the interface with a weak coupling efficiency [23]. Therefore, it is meaningful to develop mode matching techniques to coupling LW modes with higher efficiency in order to further implement these impedance-interface waveguides into systems.

Coupling techniques based on interference theory or adiabatic gradual changes are widely used to solve coupling tasks between different waveguides. Interference-based methods utilize multiple reflections in several matching stages, where destructive interference of reflected waves are achieved [27–30]. The physical size of each matching stage determines the working frequency. Thus, a main concern to utilizing these interference-based approaches is the limited working bandwidth. Gradual changes, also known as adiabatic transitions, slightly modify the structure between two different modes [31–33]. Passing through these structures, initial modes gradually transform into the target modes with low reflection within a wide bandwidth. When the unperturbed waveguides have continuous structure, the adiabatic condition could be fulfilled easily by continuously varying the waveguide structures along the propagation direction. However, when facing a complex waveguide with periodically distributed unit cells at the subwavelength scale, it is not clear how one could achieve the required smooth transitions. In the past, pioneers have solved matching tasks between guided modes in photonic waveguides[34, 35], spoof surface plasmons [5, 9, 36], as well as surface waves on arbitrary impedance surfaces [37].

In this work, adiabatic matching transitions between conventional transmission lines, a slotline and a coplanar waveguide (CPW), and a 1D

TE/TM impedance-interface waveguide is proposed. The smooth bridge consists of gradually changing TE/TM impedance surfaces and flaring ground plane, matching the momentum and impedance of the TEM mode and the LW mode. Samples are fabricated and measured. Simulated and measured S-parameters, near-field distributions, as well as the dispersion diagram demonstrate the existence of the LW mode after adiabatic transitions. Our research paves the way to implement LW modes into systems with hybrid guiding structures. Although the proposed designs operate at microwave bands, some recent work on LW modes based on plasmonic and flat graphene structures has been reported at higher frequency bands [22, 26]. Therefore, the proposed methodology can also open a door to develop mode matching techniques in integrated circuits at terahertz and optical bands.

RESULTS AND DISCUSSION

A. Physical concept of the LW mode

As shown in Fig. 1, we start by briefly introducing LW modes. Additional details about LW modes have been discussed before [23]. An electromagnetic mode can be supported by an impedance surface with an exponential decay $e^{-\alpha y}$ away from the surface and a propagation function $e^{-j\beta z}$. The surface impedances for TE and TM polarized waves are [18, 24, 37]

$$Z_{\mathrm{TE}} = -j\eta_0 \frac{k}{\alpha} \tag{1}$$

$$Z_{\mathrm{TM}} = j\eta_0 \frac{\alpha}{k} \tag{2}$$

where η_0 is the intrinsic impedance of free space, k is the wave number in free space, and α is the decay rate away from the surface. At a perfect electric and magnetic boundary condition, the tangential electric and magnetic fields vanish separately. Thus, only the TE and TM surface modes exist and the hybrid localized mode, the LW mode, appears at the interface of two surfaces with different impedances. Using cylindrical coordinates, the wave form of the LW mode can be deduced based on Bessel functions as below,

$$E_{\mathrm{z}} = E_0 K_{\frac{1}{2}}(\alpha\rho)\sin\left(\frac{\varphi}{2}\right)e^{-j\beta z} \tag{3}$$

$$H_{\mathrm{z}} = \frac{E_0}{\eta_0} K_{\frac{1}{2}}(\alpha\rho)\cos\left(\frac{\varphi}{2}\right)e^{-j\beta z} \tag{4}$$

Fig. 1 clearly indicates features of the electric field of the LW mode. The field decays away from the interface at different angles with a similar rate. Note that the electric field on the Z_{TM} surface has a strong component towards the y-axis, and the electric field on the Z_{TE} surface has strong components towards the x-axis, while at the inteterface, the electric field shows a rotational distribution.

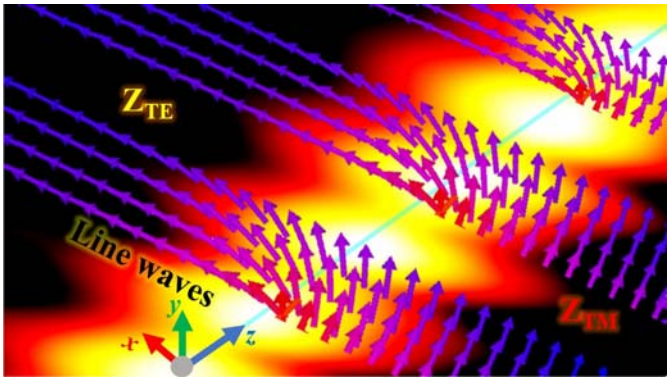

Fig. 1. The schematic of the line wave mode propagating along the interface between Z_{TE} and Z_{TM} impedance surface, arrows represent electric vectors. Metallic patches (grids) are designed to realize Z_{TE} (Z_{TM}) impedance surface.

B. Adiabatic transistions between the slotline and the impedance-interface waveguide

According to the field distribution characteristics at the interface of two impedance surfaces, it is natural to choose the TEM mode supported by a slotline as the unperturbed original mode. The electric fields of both modes at the interface are distributed along x-o-y plane. The main difference is the field penetrating into both sides of the impedance sufaces, which could be matched smoothly. In quantum physics, when the Hamiltonian of a system changes slowly, eigenmodes at any instant of time can be adiabatically transformed into another different eigenmode at a later time. Similar concepts can be applied in the electromagnetic field, when the geometry of a waveguide is gradually changed along the propagation direction, the fundamental mode can be adiabatically changed into another fundamental mode with a slightly different field distribution. Using this concept, we design a transition to match the slotline to the TE/TM impedance-interface waveguide, as shown in Fig. 2. The transition is designed to have a flaring ground plane on one side, described as $x = C_1 e^{az} + C_2$ where $C_1 = \frac{x_2 - x_1}{e^{az_2} - e^{az_1}}$ and $C_2 = \frac{x_1 e^{az_2} - x_2 e^{az_1}}{e^{az_2} - e^{az_1}}$, a = 0.1, and (z_1, x_1) and (z_2, x_2) are the starting and ending points respectively. The total length of the structure L_1 is 240 mm, the length of transitions L_{T1} is 76 mm, the length of the interface waveguide L_{LW1} is 88 mm, total width W_1 is 32 mm, the slot width S_1 is 0.08 mm, the patch width W_{S1} is 4 mm. We design periodic grid and patch arrays to realize inductive and capacitive response, supporting TM and TE modes, respectively as labeled in Fig. 2. The lattice constant p is 4 mm, the geometric parameters of the unit cells d and g are 1.8 mm and 2.8 mm, respectively. The substrate is 0.8 mm thick Rogers 5880 whose permittivity is 2.2 with 0.035 mm thick copper above it.

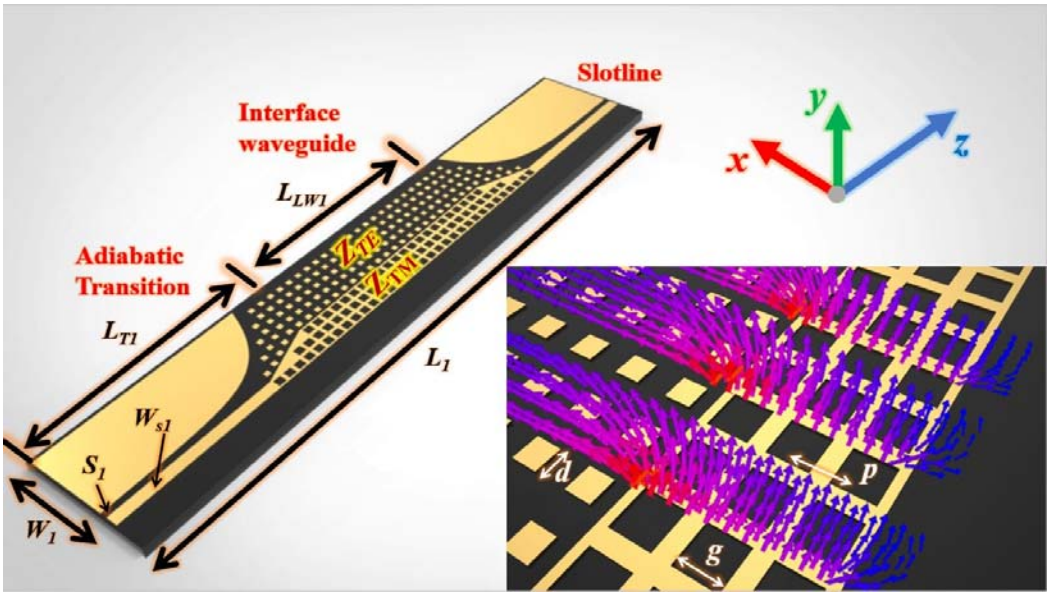

Fig. 2. Schematic of adiabatic transitions between a slotline and a TE/TM impedance interface waveguide (LW guide), where the inset shows the detail of the structure and the electric field vector distribution characteristic.

We show the simulated S-parameters of the proposed structures in Fig. 3. As a comparison, results of strucures without adiabatic transitions (connecting the slotline with the interface waveguide directly) are also shown. Without adiabatical transitions, most energy is reflected back at the abrupt connections with very low transmission efficiency. While using the adiabatic transitions, the reflection is suppressed and the transmission efficiency is increased dramatically, proving the smooth transformation from the TEM mode to the LW mode by adiabatic perturbation.

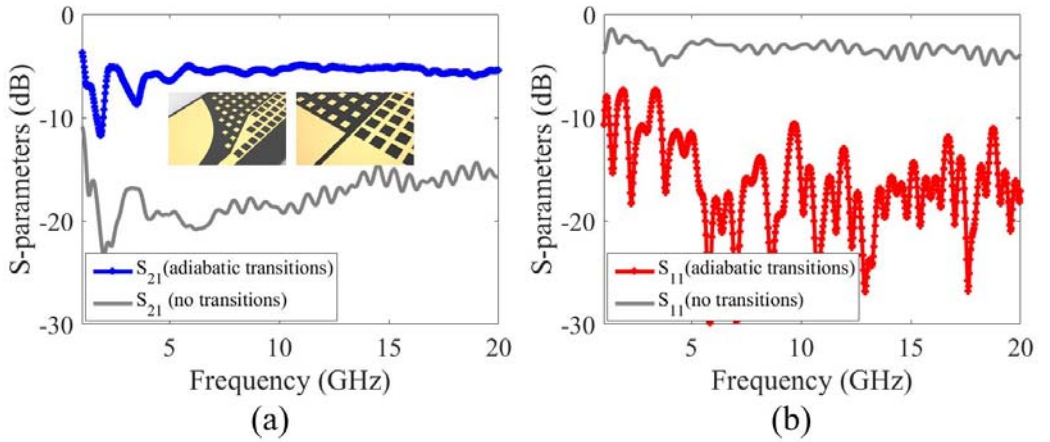

Fig. 3. (a) Simulated S_{21} and (b) S_{11} with and without adiabatic transitions between slotline and LW guide.

S-parameters measured by a network analyzer (Agilent Technologies E5071) are shown in Fig. 4. At low frequencies, simulations and measurements match well, but as the frequency increases the transmission efficiency decreases gradually due to errors likely brought on by fabrication tolerances. In order to achieve the 50 ohm characteristic impedance of the slotline, the width of the slot is only 0.08 mm, and the impedance is very sensitive when soldered to the connectors, especially at high frequencies.

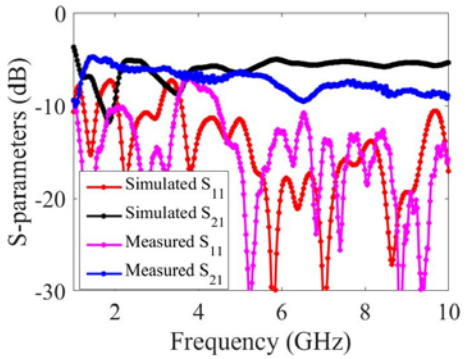

Fig. 4. S-parameters of the slotline/LW guide.

Although only S-parameters below 10 GHz are presented due to the limitation of connectors, we could still further esitimate field distributions at higher frequency band within the desirable area, ignoring the reflection loss from connectors on both sides. Fig. 5 (a) shows the photograph of the near-field scan. One port of the sample is connected to a broadband matching load and the other port of the sample is connected to the first port of the network analyzer whose second port is connected to the electric probe driven by a motor to scan the target area. Measured and simulated electric field distributions at 6 GHz and 20 GHz are shown in Fig. 5 (b-e). It is difficult to discern the LW mode at 6 GHz from measurements, while the simulated profile of total electric field indicates the existence of the LW mode along the 1D inteterface. In order to better understand the difference, investigating the electric vector distributions of the LW mode in Fig. 2 is instructive. The probe detects electric field primarily towards the y-axis. Therefore, more energy above the TM impedance surface with a mainly y-axis polarized electric vector field will be detected than above the TE impedance surface with mainly x-axis polarized electric field. This makes it more difficult to identify the LW mode at the 1D interface through experiments, especially at low frequencies when the decay rate into both sides remains low. It should also be mentioned that the transition acts as a plannar horn antenna. Thus, part of the energy is radiated out during the adiabatic procedure, which is the main cause of the transmission loss.

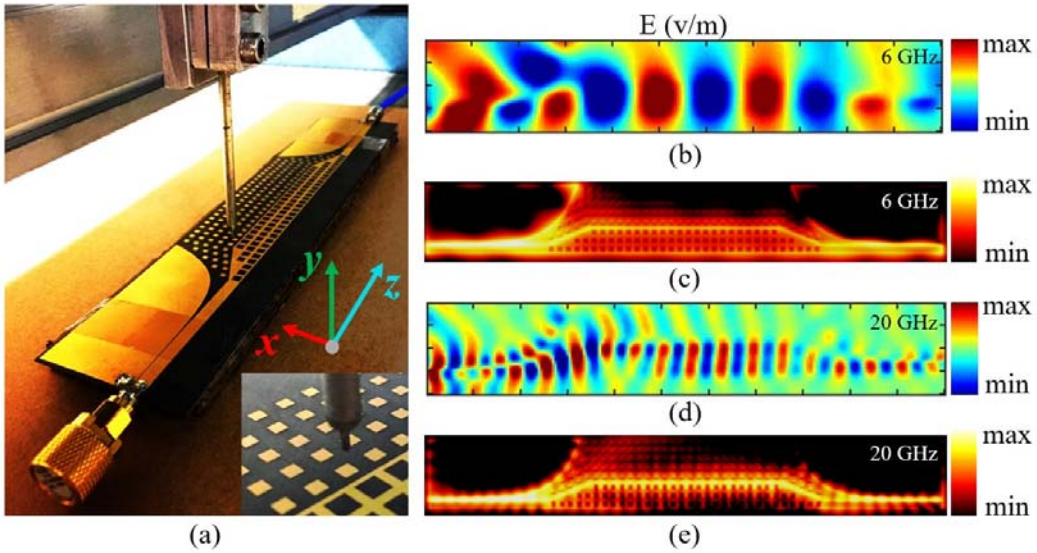

Fig. 5. (a) The photograph of the near-field scan where the electric probe was positioned 1 mm above the sample, and the inset at the corner shows the detail of probe. (b) Measured E_z distributions at 6 GHz. (c) Simulated electric field distributions at 6 GHz. (d) Measured E_z distributions at 20 GHz. (e) Simulated electric field distributions at 20 GHz.

C. Adiabatic transistions between the CPW and the impedance-interface waveguide

In order to suppress the radiation loss, it is natural to consider designing a symmetric structure with field distributed in opposite directions during the adiabatic procedure. The TEM mode of a CPW is an ideal candidate as the starting unperturbated state. The structure is shown in Fig. 6. The width W_{S2} is 4 mm and width of slot S_2 is 0.17 mm, other geometric parameters are the same with the slotline/LW design. The adiabatic transitions are the same as transitions discussed previously. At the middle section, there is a sandwich-like structure consisting of TE/TM/TE impedance surfaces where two mirror-symmetric LW modes will be transported along two 1D impedance-interface waveguides. The electric field vector distribution characteristic of the sandwich-like structure is shown in the inset.

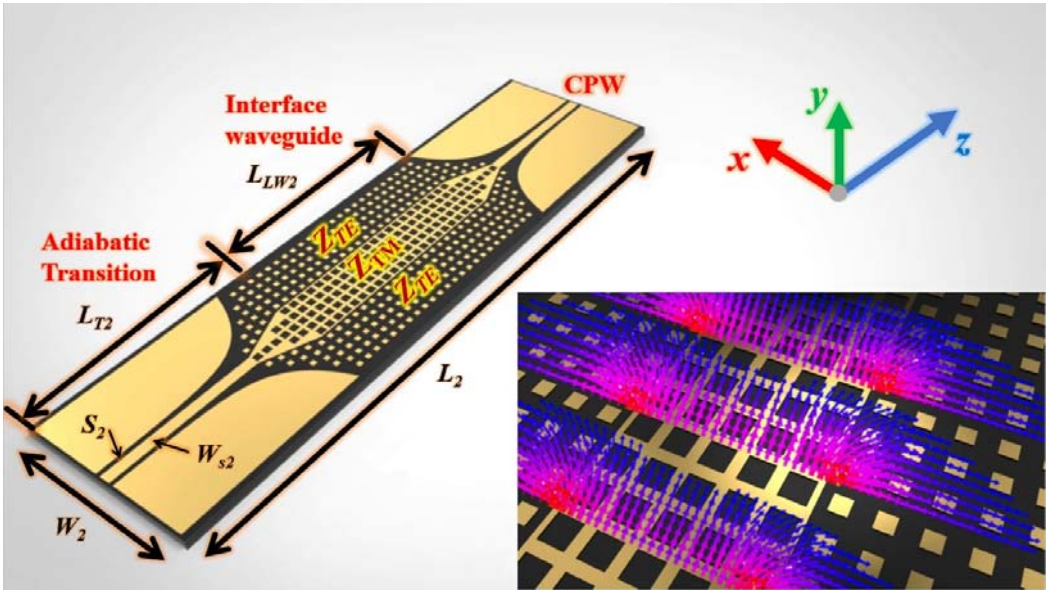

Fig. 6. Schematic of the adiabatic transition between a CPW and a LW guide, where the inset shows the detail of the structure and the electric vector distribution characteristic.

The measured and simulated S-parameters are shown in Fig. 7(a) and we further compare it with the proposed slotline/LW guide structure in Fig. 7(b). Due to the suppression of radiation loss from transistions, the CPW-LW structure show higher transimission efficiency.

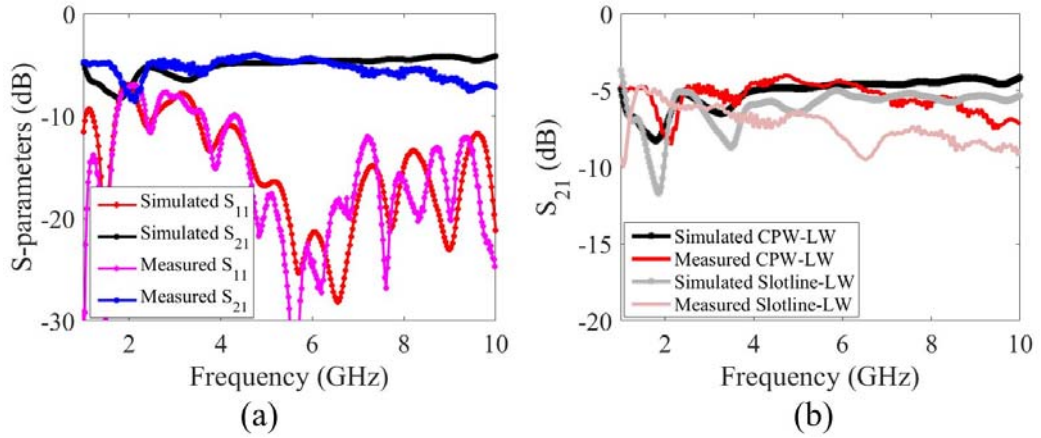

Fig. 7. (a) Simulated and measured S-parameters of the CPW/LW guide. (b) Comparisons of S_{21} between CPW/LW and slotline/LW guides.

We also conducted a near-field scan at 6 GHz and 20 GHz, as shown in Fig. 8. Simiar to previous results in Fig. 5, it is somewhat difficult to recoginize the LW mode at 6 GHz, for the same reason as explained before. However, through simulations, we can analyze the total electric field to verify the existence of the LW mode. We also use the Fourier transform to analyze the near-field distribution every 0.5 GHz from 1GHz

to 20 GHz to obtain the dispersion diagram of the LW mode in Fig. 9, where eigenmode simulated results are also ploted as a comparison. The results match well, further proving the existence of the LW mode.

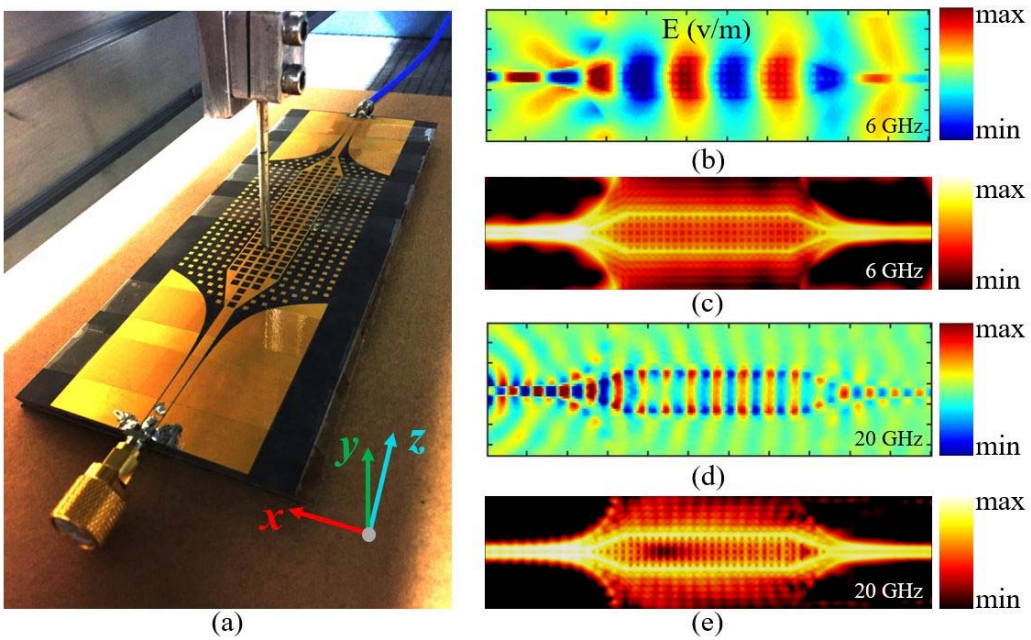

Fig. 8. (a) The photograph of a near-field scan where the electric probe was positioned 1 mm above the sample, and the inset at the corner show the detail of probe. (b) Measured E_z distributions at 6 GHz. (c) Simulated electric field distributions at 6 GHz. (d) Measured E_z distributions at 20 GHz. (e) Simulated electric field distributions at 20 GHz.

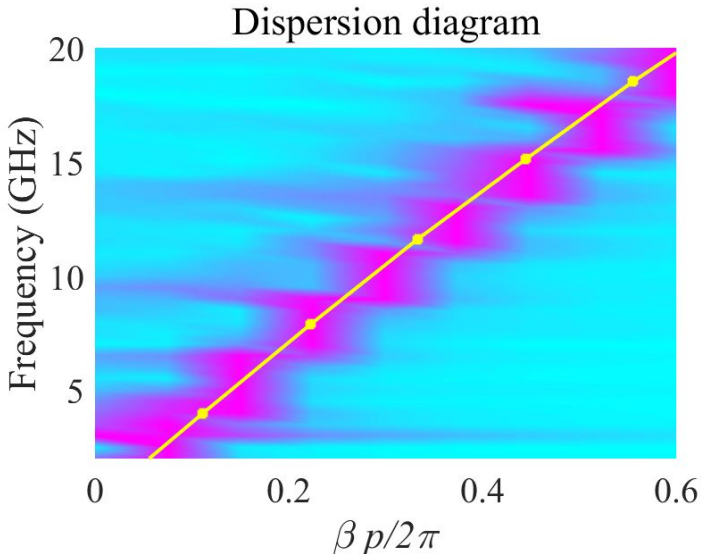

Fig. 9 The dispersion diagram of the LW mode, where the background is deduced by Fourier transform of measured near-field distributions and the yellow line is simulated results from eigenmode solver.

CONCLUSION

To sum up, the work shows that the principle of adiabatic matching can be used to design transitions for transform TEM modes, which are common modes in traditional waveguides, into the recently discovered LW modes at a 1D interface of artificial impedance surfaces. Two matching tasks starting from CPW and slotline are provided as examples of the technique. The proposed adiabatic matching strategy shows a high robustness in broadband applications, opening the door to implement LW modes into systems from microwave bands all the way to optical bands.

ACKNOWLEDGMENTS

This work was supported by National Natural Science Foundation of China (Nos. 61771127 and 61427801), Scientific Research Foundation of Graduate School of Southeast University (No. YBJJ1814), and Postgraduate Research & Practice Innovation Program of Jiangsu Province (No. KYCX18_0098) as well as AFOSR contract FA9550-16-1-0093.

REFERENCES

[1] J. Polo, T. Mackay, and A. Lakhtakia, *Electromagnetic Surface Waves: A Modern Perspective* (Newnes, 2013).

[2] S. A. Maier, *Plasmonics: fundamentals and applications* (Springer Science & Business Media, 2007).

[3] J. D. Jackson, *Classical Electrodynamics* (Wiley, New York, 1962).

[4] R. B. M. Schasfoort, *Handbook of Surface Plasmon Resonance: 2nd Edition* (Royal Society of Chemistry, 2017).

[5] S. Laurette, A. Treizebre, and B. Bocquet, Corrugated Goubau Lines to Slow Down and Confine THz Waves, *IEEE Trans. Terahertz Sci. Technol.*, **2**, 340 (2012).

[6] G. Goubau, Open Wire Lines, *IRE Trans. Microw. Theory Tech.*, **4**, 197 (1956).

[7] G. Goubau, Waves on interfaces, *IRE Trans. Antennas Propag.*, **7**, 140 (1959).

[8] J. B. Pendry, L. Martín-Moreno, and F. J. Garcia-Vidal, Mimicking surface plasmons with structured surfaces, *Science*, **305**, 847 (2004).

[9] H. F. Ma, X. Shen, Q. Cheng, W. X. Jiang, and T. J. Cui, Broadband and high-efficiency conversion from guided waves to spoof surface plasmon polaritons, *Laser Photonics Rev.*, **8**, 146 (2014).

[10] W. L. Barnes, A. Dereux, and T. W. Ebbesen, Surface plasmon subwavelength optics, *Nature*, **424**, 824 (2003).

[11] Z. Xu, S. Li, X. Yin, H. Zhao, and L. Liu, Radiation loss of planar surface plasmon polaritons transmission lines at microwave frequencies, *Sci. Rep.*, **7**, 6098 (2017).

[12] E. A. J. Marcatili, Dielectric Rectangular Waveguide and Directional Coupler for Integrated Optics, *Bell Syst. Tech. J.*, **48**, 2071 (1969).

[13] Y. G. Smirnov and D. V. Valovik, Guided electromagnetic waves propagating in a plane dielectric waveguide with nonlinear permittivity, *Phys. Rev. A*, **91**, 013840 (2015).

[14] U. Langbein, F. Lederer, and H.-E. Ponath, Generalized dispersion relations for nonlinear slab-guided waves, *Opt. Commun.*, **53**, 417 (1985).

[15] D. Mihalache, M. Bertolotti, and C. Sibilia, in *Progress in Optics* (Elsevier, 1989), vol. 27, pp. 227–313.

[16] U. Langbein, F. Lederer, T. Peschel, U. Trutschel, and D. Mihalache, Nonlinear transmission resonances at stratified dielectric media, *Phys. Rep.*, **194**, 325 (1990).

[17] A. D. Boardman, P. Egan, F. Lederer, U. Langbein, and D. Mihalache, in *Modern Problems in Condensed Matter Sciences*, H.-E. Ponath, G. I. Stegeman, Eds. (Elsevier, 1991), vol. 29 of *Nonlinear Surface Electromagnetic Phenomena*, pp. 73–287.

[18] D. Sievenpiper, L. Zhang, R. F. J. Broas, N. G. Alexopolous, and E. Yablonovitch, High-impedance electromagnetic surfaces with a forbidden frequency band, *IEEE Trans. Microw. Theory Tech.*, **47**, 2059 (1999).

[19] J. D. Joannopoulos, P. R. Villeneuve, and S. Fan, Photonic crystals, *Solid State Commun.*, **102**, 165 (1997).

[20] M. Z. Hasan and C. L. Kane, Colloquium: Topological insulators, *Rev. Mod. Phys.*, **82**, 3045 (2010).

[21] A. B. Khanikaev, S. Hossein Mousavi, W.-K. Tse, M. Kargarian, A.

H. MacDonald, and G. Shvets, Photonic topological insulators, *Nat. Mater.*, **12**, 233 (2013).

[22] D. R. Mason, S. G. Menabde, S. Yu, and N. Park, Plasmonic Excitations of 1D Metal-Dielectric Interfaces in 2D Systems: 1D Surface Plasmon Polaritons, *Sci. Rep.*, **4**, 4536 (2014).

[23] D. J. Bisharat and D. F. Sievenpiper, Guiding Waves Along an Infinitesimal Line between Impedance Surfaces, *Phys. Rev. Lett.*, **119**, 106802 (2017).

[24] X. Kong, D. J. Bisharat, G. Xiao, and D. F. Sievenpiper, Analytic theory of an edge mode between impedance surfaces, *Phys. Rev. A*, **99**, 033842 (2019).

[25] E. Martini, M. G. Silveirinha, and S. Maci, Exact Solution for the Protected TEM Edge Mode in a PTD-Symmetric Parallel-Plate Waveguide, *IEEE Trans. Antennas Propag.*, **67**, 1035 (2019).

[26] D. J. Bisharat and D. F. Sievenpiper, Manipulating line waves in flat graphene for agile terahertz applications, *Nanophotonics*, **7**, 893 (2018).

[27] T. Baba and D. Ohsaki, Interfaces of Photonic Crystals for High Efficiency Light Transmission, *Jpn. J. Appl. Phys.*, **40**, 5920 (2001).

[28] J. Witzens, M. Hochberg, T. Baehr-Jones, and A. Scherer, Mode matching interface for efficient coupling of light into planar photonic crystals, *Phys. Rev. E*, **69**, 046609 (2004).

[29] H. Iizuka and N. Engheta, Antireflection structure for an effective refractive index near-zero medium in a two-dimensional photonic crystal, *Phys. Rev. B*, **90**, 115412 (2014).

[30] Z. Yao, J. Luo, and Y. Lai, Photonic crystals with broadband, wide-angle, and polarization-insensitive transparency, *Opt. Lett.*, **41**, 5106 (2016).

[31] E. Verhagen, M. Spasenović, A. Polman, and L. (Kobus) Kuipers, Nanowire Plasmon Excitation by Adiabatic Mode Transformation, *Phys. Rev. Lett.*, **102**, 203904 (2009).

[32] B. Momeni and A. Adibi, Adiabatic matching stage for coupling of light to extended Bloch modes of photonic crystals, *Appl. Phys. Lett.*, **87**, 171104 (2005).

[33] R. Dangel, A. L. Porta, D. Jubin, F. Horst, N. Meier, M. Seifried, and B. J. Offrein, Polymer Waveguides Enabling Scalable Low-Loss Adiabatic Optical Coupling for Silicon Photonics, *IEEE J. Sel. Top. Quantum Electron.*, **24**, 8200211 (2018).

[34] Y. Xu, R. K. Lee, and A. Yariv, Adiabatic coupling between conventional dielectric waveguides and waveguides with discrete translational symmetry, *Opt. Lett.*, **25**, 755 (2000).

[35] S. G. Johnson, P. Bienstman, M. A. Skorobogatiy, M. Ibanescu, E. Lidorikis, and J. D. Joannopoulos, Adiabatic theorem and continuous coupled-mode theory for efficient taper transitions in photonic crystals, *Phys. Rev. E*, **66**, 066608 (2002).

[36] A. Kianinejad, Z. N. Chen, and C. Qiu, Design and Modeling of Spoof Surface Plasmon Modes-Based Microwave Slow-Wave Transmission Line, *IEEE Trans. Microw. Theory Tech.*, **63**, 1817 (2015).

[37] J. Lee and D. F. Sievenpiper, Patterning Technique for Generating Arbitrary Anisotropic Impedance Surfaces, *IEEE Trans. Antennas Propag.*, **64**, 4725 (2016).